IIETA International Information and Engineering Technology Association
Advancing the World of Information and Engineering

Journal of New Materials for Electrochemical Systems
Vol. 27, No. 3, September 2024, pp. 163-171
Journal homepage: http://iieta.org/journals/jnmes

Study on Electrochemical Stability and Charge Transfer Efficiency for the Development of High-Performance Supercapacitors Using Iron Oxide (Fe_2O_3) Nanorods

Vijay Ramrao Khawale[1], Mayank[2], Ravi Kumar[3], P. Satishkumar[4*], Barun Haldar[5], B. Deepa[6], Rajasekaran Saminathan[7], P. Veeramanikandan[8], Azhagu Saravana Babu Packirisamy[9], Mayakannan Selvaraju[4]
,
[1]Department of Mechanical Engineering, Yeshwantrao Chavan College of Engineering, Nagpur, Maharashtra, India.
[2]Bio-Chemical Engineering Department, BTKIT Dwarahat, Almora, Uttrakhand, India.
[3]Mechanical Engineering Department, BTKIT Dwarahat, Almora, Uttrakhand, India
[4*]Department of Mechanical Engineering, Rathinam Technical Campus, Coimbatore, Tamil Nadu, India
[5]Industrial Engineering Department, College of Engineering, Imam Mohammad Ibn Saud Islamic University (IMSIU), Riyadh-11432, Kingdom of Saudi Arabia.
[6]Department of Science and Humanities, Karpagam Academy of Higher Education, Coimbatore, Tamilnadu 641 021
[7]Department of Mechanical Engineering, College of Engineering and computer science, Jazan University, Saudi Arabia.
[8]Department of Electrical and Electronics Engineering, Dhanalakshmi Srinivasan college of Engineering and Technology, Mahabalipuram, Chennai, India
[9]Department of Biotechnology, Vel Tech Rangarajan Dr.Sagunthala R&D Institute of Science and Technology, Chennai-600062, India

Corresponding Author Email: sp.sathishkumar10@gmail.com

https://doi.org/10.14447/jnmes.v27i3.a01

Received: 12/01/2024
Accepted: 16/08/2024

Keywords:
Charge–discharge cycles, Permeable Fe2O3 nanorods,Specific capacitance, Effectiveseriesresistance,Electrochemicalsuper capacitors

ABSTRACT

A novel electrode material for electrochemical supercapacitors is introduced in this study: hydrothermally produced permeable iron oxide (Fe2O3) nanorods (NRs). The Fe2O3 nanorods exhibit exceptional crystallinity and phase purity, and X-ray diffraction (XRD) studies validated their cubic crystalline structure inside an Ia3 space collective. An examination of the morphology of the Fe2O3 NRs uncovered their nanostructured characteristics, such as a rod-shaped structure with an average dimension of about 30 nm. A record specific capacitance of 489 F/g was attained by conducting electrochemical performance studies using Fe2O3 NRs electrodes for supercapacitors at 10 mVs-1scan rate. The effective series resistance (ESR) was determined using electrochemical impedance spectroscopy (EIS). It measured 3.26 Ω, indicating a low resistance and efficient charge transport kinetics. Fe2O3 NRs electrodes exhibited exceptional chemical stability, maintaining excellent capacitance even after 500 charge-discharge cycles at a current density of 6 Ag-1. This study presents a scalable method for creating high-performance supercapacitors using Fe2O3 NRs to improve the development and design of upcoming energy storage devices.

1. INTRODUCTION

There has been a mad dash to find new ways to store and convert energy due to the ever-increasing demand for it and growing worries about the sustainability of conventional energy sources. Because renewable power output is not always consistent, energy storage is essential in this context for meeting modern energy demands. In the pursuit of better energy management and usage, a great deal of research and development has gone into two primary forms of energy storage: batteries and supercapacitors [1], [2].

The ever-increasing need for energy is putting a heavy burden on batteries, a well-established technology for energy storage. For instance, there are a number of major drawbacks to lithium-ion batteries that are so pervasive despite their widespread use: a low power density, a short lifespan, safety concerns and a dependence on finite lithium resources. These factors make them inefficient when it comes to storing big amounts of energy [3], [4].

Supercapacitors are a novel and perhaps revolutionary kind of energy storage technology due to its capacity to provide huge power outputs in comparatively short durations of time [5]. There are a lot of advantages to using supercapacitors, such as the fact that they are environmentally friendly, last a long time, work in a wider range of temperatures, and have exceptional power densities. A lot of people are interested in supercapacitors (SCs) since they are a great energy storage option with many great features, including as a long cycle life, low cost, safety, specific capacity, and high-power density. A supercapacitor's versatility stems from its exceptional capacity to swiftly release electrical energy [6], [7], [8]. They can be utilized autonomously or in conjunction with batteries to supply extra power as necessary. They are beneficial for applications requiring quick energy discharge and recharge cycles, as they may link high-power demand with inconsistent energy sources. Supercapacitors' energy storage technologies mainly fall into two categories: pseudo-capacitors and electrical double-layer capacitors (EDLC)[9]. The reported

capacitance in pseudo-capacitors is due to faradic processes that involve electro-active species within the electrode material. These species could be surface functional groups or transition metal oxides. Because of their role in reversible redox reactions, these species improve electrical energy storage capabilities. The selection of electrode materials is a significant focus of supercapacitor research and development since it defines their capabilities and efficiency [10], [11], [12]. As a rule, the electrode materials of supercapacitors include carbon-based materials, conducting polymers, oxides of transition metals, and comparable compounds. Attractive electrode materials for supercapacitors include transition metal oxides due to their widespread availability, low cost and high redox activity [13], [14]. Cobalt oxide (Co_3O_4), ruthenium dioxide (RuO_2), vanadium pentoxide (V_2O_5), Nickel oxide (NiO), titanium dioxide (TiO_2), iron dioxide (Fe_2O_2) and molybdenum trioxide (MoO_3) are all instances of transition metal oxides presented in the literature [15], [16], [17]. Because of their exceptional electrochemical properties and redox capacities, they have garnered interest in enhancing the performance of supercapacitors [18], [19].

Iron oxide and similar oxides are among the most promising materials among the various metal oxides available for use as electrodes in supercapacitors. For instance, Fe_2O_3 has remarkable physical and chemical stability over a range of electrolytes, is non-toxic, and can be architecturally bent to suit different needs. Because of its durability and lack of environmental impact, Fe_2O_3 is a great material for supercapacitor electrodes. Despite being compatible with both acidic and alkaline electrolytes, there is still a lot of untapped potential for improving the capacity and energy storage capacities of electrodes based on Fe_2O_3[20], [21], [22].

Chemical advancements, integration with conductive materials having a high surface area and the creation of nanostructures are only a few examples of the many optimization efforts that have been applied to electrodes based on Fe_2O_3. By capitalizing on Fe_2O_3's inherent strengths and mitigating its potential weaknesses, these endeavors aim to enhance the material's performance as an electrode substance for supercapacitors [23], [24]. Due to its limited porosity, low ionic conductivity, unstable morphology, and lack of cyclic stability, Fe_2O_3 supercapacitor electrodes have not achieved success thus far. An increase in Fe_2O_3 due to the development of cyclic stability reduced the efficiency of the supercapacitor devices. In order to make Fe_2O_3 a potent material for supercapacitor electrodes, many ways have been devised to overcome these constraints. To get the most out of Fe_2O_3 in materials used as supercapacitor electrodes, it's best to increase the particular surface area and change the morphological properties[25], [26], [27].

This work focuses on the production of permeable Fe_2O_3 nanorods using hydrothermal methods for application in supercapacitors. We plan to do a thorough examination of the electrochemical behavior and efficiency of these permeable Fe_2O_3 NRs to find out if they are good electrode materials for supercapacitors. To contribute to ongoing endeavors to enhance supercapacitor technology and address the growing challenges of contemporary energy storage, we want to illuminate their electrochemical characteristics and capacities.

2. EXPERIMENTAL METHODOLOGY OF PERMEABLE FE_2O_3 NANORODS

2.1 Fabrication and Descriptions

Iron oxide (Fe_2O_3) nanorods (NRs) were meticulously synthesized according to a well-designed technique as part of our investigative efforts. The synthesis procedures and ingredients are detailed below:

A solution containing 5 mM iron acetate ($Fe(CH_3CO_2)_2$, Sigma-Aldrich) and 2.5 mM $C_2H_2O_4$ in 100 ml of deionized water is used in composition of the iron oxide nanorod at work. The solution turned a very brown color first, but its pH was reduced to 10 by adding a 2 M NaOH solution. The solution changed color from a light brown to a darker brown due to the pH change. A tightly sealed Teflon beaker was used to transfer the reaction suspension in order to carry out the hydrothermal reaction. The reaction was then carried out at a temperature of 120ºC for a duration of 16 hours. Filtration was used to properly recover the precipitates once the autoclave had cooled to the proper temperature. The obtained precipitates were removed using a three-stage washing technique including ethanol and DI water. Afterwards, the precipitates were left to dry overnight in an oven set at 80ºC. Following that, a three-hour calcination procedure was performed at 350ºC to remove residual impurities, yielding in creation of dark, delicately powdered material. The Mn(CH3CO2)2 precursor, in its as-prepared state, was heated further to produce Fe_2O_3 nanorods using a hydrothermal procedure. We have used spectroscopic approaches to detect the as-synthesized forms of both the iron acetate precursor and the final product.

The compositional, optical, vibrational, structural, and morphological features of the produced Fe_2O_3 were investigated using a range of characterization techniques. This made it possible to characterize the material in great detail. The crystal structures and phases of the generated composite were revealed through the use of XRD Bruker D8 ADVANCE examination at a 10-80º diffracting angle with Cu-Kα radiation (λ= 1.54 Å). Researchers utilized Raman spectroscopy to find contaminants and flaws in the structure of the permeable Fe_2O_3 NRs. A Hitachi-Japan S-3000H apparatus was utilized for the investigation. Using the 400cm^{-1} to 4000 cm^{-1} range of the Fourier transform infrared spectroscopy (FTIR)-VERTEX 70, we investigated the vibrational characteristics and chemical interactions. It is possible to compress the synthetic material with milled KBr (1wt%) and place it on a pallet in order to prepare it for FTIR tests. Because it could interfere with the procedure if it was still damp, the KBr was dehydrated at 100ºC in an air oven before use.

2.2 Electrochemicalanalysis

A sequence of examinations was conducted at room temperature to evaluate the electrochemical performance of the produced Fe_2O_3 NRs. The experiment employed a three-electrode cell arrangement and electrochemical analysis. A functional electrode was created by thoroughly mixing finely ground Fe_2O_3 NRs, polyvinyl fluoride (PVDF) binder and acetylene black in a precise weight ratio of 85:10:05. The ingredients were combined with the N-methyl pyrrolidone (NMP) solvent to create a homogeneous paste. The material

was cured in a hot air oven at 80ºC for 12 hours after being utilized to a 1 × 1 cm^2 nickel foam substrate. The Fe_2O_3 NRs composite's working electrodes were constructed using NF substrates. The experiment utilized a platinum wire counter electrode and an aqueous electrolyte solution containing 1 M KOH as the reference and counter electrodes, respectively. The active ingredient was utilized in a milligram form. In order to gain aimproved understanding of the performance characteristics and potential suitability of the generated Fe_2O_3 NRs as electrode materials for supercapacitors, we conducted electrochemical performance tests in strict accordance with experimental protocols.

3. RESULTS AND DISCUSSIONS

3.1 Classifications and its properties of permeable Fe_2O_3NRs

The structural properties of the produced permeable Fe_2O_3 nanorods (NRs) were thoroughly examined utilizing XRD analysis, which provided valuable information about the material's crystallographic features. The XRD pattern appears to have distinct diffraction peaks at 19.4°, 26°, 34.8°, 39.3°, 46.4º, 55.9º, and 66.6° 2θ angles, as shown in Figure 1(a). Peaks at 200, 211, 222, 400, 332, 440, and 622 nm, respectively, represent the crystallographic planes of Fe_2O_3[28], [29], [30]. The found peaks clearly show the cubic phase structure of Fe_2O_3 with unit cell factors = 9.5Å, which belongs to the space group Ia3.

The FTIR analysis was used to study the chemical make-up, chemical bonding characteristics, and purity of the substance. The Fe_2O_3 NRs sample's FTIR spectra, spanning 400 to 4000 cm^{-1}, are displayed in Figure 1(b). Peaks and characteristics can be seen in the infrared spectra obtained by using the Fourier transform. When water molecules are present, a strong signal at about 3450 cm^{-1} shows the existence of hydroxyl (OH) groups. Possibility of a peak at 1670 cm^{-1} provides additional proof of C-C stretching. Alcohol molecules' C-H and O-H bond stretching are associated with two peaks at 1520 and 1392 cm^{-1}respectively. Two significant infrared peaks at 705 and 612 cm^{-1}further confirm the occurrence of Mn-O stretching vibrations [31].

Raman spectroscopy was utilized to examine the crystalline characteristics and potential structural alterations of the Fe_2O_3 NRs (Fig. 1 (c)). When Fe_2O_3 NRs are synthesized, their Raman-scattering spectra take on distinctive features. A strong Raman band is present at 651 cm^{-1} while2smaller and weaker bands may be found at 389 cm^{-1} and 508 cm^{-1}. The Raman band at 668 cm^{-1} and stretching bridge Mn-O-Mn caused by the Ia3 crystal structure of Fe_2O_3. The 2 weak Raman bands at 389 and 508 cm^{-1} respectively in Fe_2O_3 and its companion compounds show the presence of out-of-plane bending modes [32].
Surface area, pore volume, and internal and external specific surfaces are all enhanced when Fe_2O_3 nanorods are synthesized. The visible fine lines on the nanorods' surfaces, which represent an imperfect morphology at their corners, are the source of these increases. Because of their distinct structural properties, Fe_2O_3 nanorods should work exceptionally well as electrode materials in supercapacitor systems.

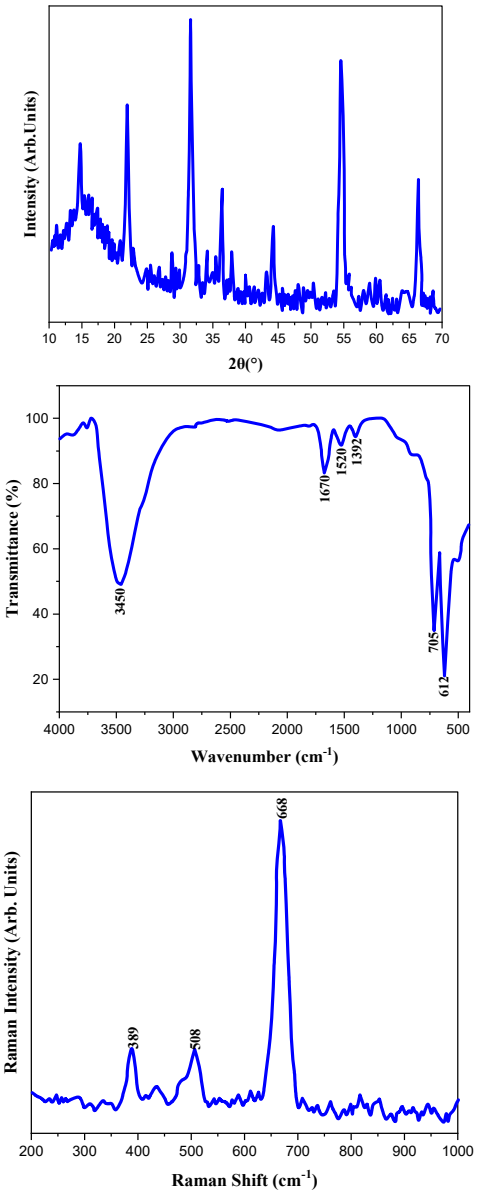

Figure 1. As synthesized hollowFe_2O_3nanorods(a)Raman-scattering spectrum(b) XRDpattern (c) FTIRspectrum.

The formation of the distinctive structure of permeable Fe_2O_3 nanorods during their hydrothermal production procedure relies on a number of chemical reactions. Here is a comprehensive breakdown:

$$Fe(CH_3COO).2H_2O \rightarrow Fe^{2+} + 2CH_3COO^- + 2H_2O \quad (1)$$

$$2Fe^{2+} + 5OH^- \rightarrow Fe(OH)_2 + 2Fe(OH)_3 \quad (2)$$

$$Fe(OH)_2 + 2Fe(OH)_3 \xrightarrow[3h]{350^{\circ}C} Fe_2O_3 + 4H_2O \quad (3)$$

To separate iron and acetate ions from iron acetate, a basic medium is utilized. Iron trihydroxide and iron dihydroxide are the by products of a reaction with hydroxide ions. Iron dihydroxide starts to self-assemble, turning into a distinctive rod-like shape, during the hydrothermal process, which entails heating the particles for a long duration at 120ºC. After the

hydroxide nanostructures are made, the final step is to anneal them at 350ºC for three hours. At the right temperature, iron hydroxides can have their water molecules removed, allowing them to undergo a phase transition and become permeable Fe_2O_3 nanorods. The nanorods produced display a distinct structure, verified using various characterization techniques. The generated nanorods possess intriguing features and have the potential to serve as electrochemical supercapacitors.

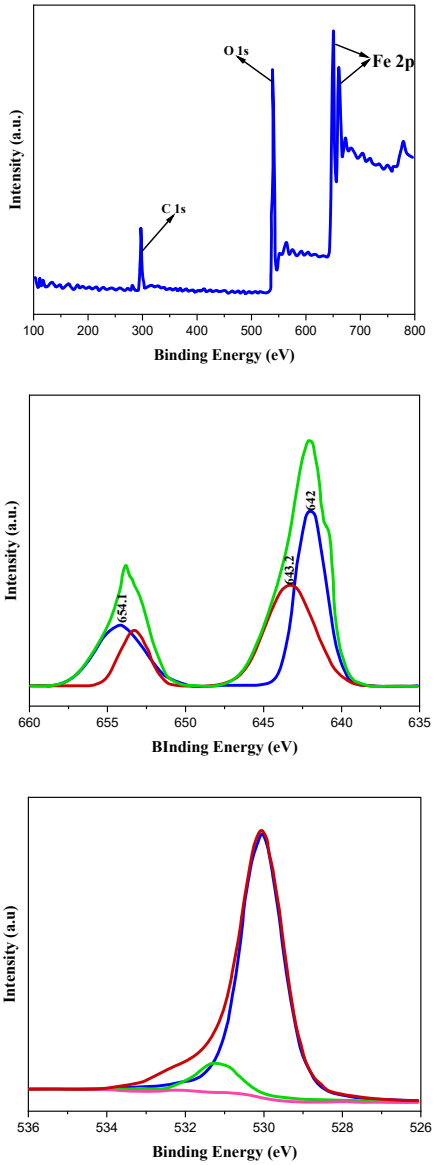

Figure 2. Binding energies of (a) Fe_2O_3 NRs' completely perused XPS spectrum, core regions (b) Fe, and (c) O.

Our produced nanorods were thoroughly examined for their chemical composition and electronic states using XPS. Figure 2shows the high-resolution XPS spectra and the findings of the analysis. The XPS survey spectra of the produced permeable Fe_2O_3 NRs are shown in Figure 2 (a). The binding energies of Mn 2p and O 1s are corresponding to two significant peaks, while a smaller peak appears to represent C 1s. This peak is probably induced by residual precursors from the synthesis. The high-resolution XPS spectra of the Mn 2p region are displayed in Figure 2 (b). The Mn 2p3/2 core region binding energies and Mn 2p1/2 core region have been determined to be 642 and 654.1 eV, respectively [33]. Since Mn 2p signals are present, it is probable that the produced permeable Fe_2O_3 NRs contain Mn3+ states. The obtained orbit splitting value of 12.1 eV is also consistent with Fe_2O_3principles found in previous studies [34]. These results validate the production of Fe_2O_3 and also show that the cubic crystal structure of Fe_2O_3 agrees with the XRD data. Fitting the O 1s X-ray photoelectron spectroscopy data to the binding energies is shown in Figure 2 (c). There are 531.22 eV for lattice oxygen binding energies with metal (O-Fe-O) and 530.05 eV for adsorbed oxygenated species, like hydroxyl (-OH) created from material surface's adsorbed moisture.

This means that the synthetic material is primarily Fe_2O_3, devoid of meaningful oxide impurities, according to the XPS results. A wide range of analytical methods have been used to characterize the synthetic permeable Fe_2O_3 NRs. Due to this, we can deduce their compositional and structural characteristics, which validates their promise as a component of energy storage devices, particularly supercapacitors.

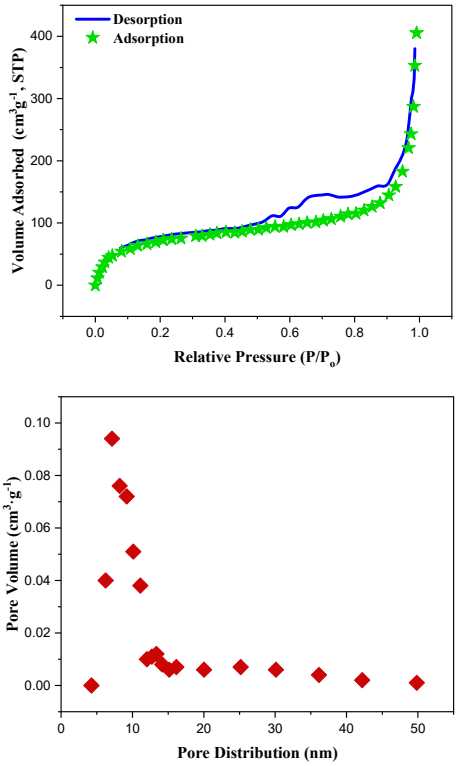

Figure 3 (a) The pore size dispersion graphs of the synthetic permeable Fe_2O_3 NRs and (b) the N2 adsorption-desorption isotherms.

As displayed in Figure 3, the surface behavior of synthetic permeable Fe_2O_3 NRs was examined by evaluating the nitrogen adsorption-desorption isotherms. A clear hysteresis loop extending from 0.5 to 0.85 relative pressure is observed in the produced permeable Fe_2O_3 NRs, which is represented by a Type II desorption - adsorption. Permeability is demonstrated by the presence of a Type II desorption - adsorption isotherm. With a predicted BET surface area of 74.6 m^2/g, the synthetic

permeable Fe_2O_3 NRs should perform admirably. So, it seems the structure allowed water to seep through. Figure 4(b) shows pore widths ranging from 5 to 14 nm, which are indicative of mesopores. Thus, Fe_2O_3 nanorods created by synthesis with high permeability can accelerate electrochemical processes.

3.2 Application of Supercapacitor of as-received permeable Fe_2O_3

Electrochemical experimenting with galvanostatic charge-discharge (GCD) and cyclic voltammetry (CV) was performed on Fe_2O_3 NRs to determine their potential as a supercapacitor electrode. The studies offered a comprehensive insight into the electrode's ability to store charge under different operating situations.

By increasing the potential window (ΔV) from -0.2 to 0.6 V, information for the CV measurements were collected at different scan rates. A precise calculation of the Fe_2O_3 electrode's specific capacitance (Csp) was performed utilizing CV datasets and data acquired from previous studies in order to assess the electrochemical performance [35]. The produced electrode's Csp was calculated using this equation.

$$C_{sp} = \frac{\int idv}{s\Delta V.m} \quad (1)$$

Equation (2) can be used to find the particular capacitance value from GCD:

$$C_{sp} = \frac{I\Delta t}{m \cdot \Delta V} \quad (2)$$

Figure 4 (a) displays individual capacitance values derived from cyclic voltammetry analysis: 489 F/g at a scan rate of 10 mVs^{-1}, 437 F/g at 40 mVs^{-1}, 279 F/g at 60 mVs^{-1}, and 182 F/g at 100 mVs^{-1}.The significant variations in redox peaks with higher scan rates proved that redox processes were the main charge-storage mechanism. The remarkable reversibility of the electrode material was demonstrated by the cyclic voltammetry curves' ability to maintain the quasi-rectangular shape even at greater scan speeds. Ion diffusion was uniform on both the inner and outer electrode surfaces at lower scan rates, but predominantly on the outer surface at higher scan rates. Interestingly, the scan rate that produced the highest specific capacitance was the one with the lowest value.

Following the addition of Fe_2O_3 NRs, we conducted a more thorough investigation of the electrode's charge-discharge behavior using GCD, an approach that is equally significant for evaluating supercapacitor performance. Visualizing the charge-discharge curves for current densities ranging from 1 to 10 Ag^{-1} and potentials spanning from 0.0 V to 0.4 V is done in Fig. 5(b). At various current densities, these profiles show how complicated the charging and discharging processes are. Research has demonstrated that at different current densities, the potential-time curves behave in an almost symmetrical fashion, suggesting a negligible polarization effect and a high charge-discharge Coulombic effectiveness[36-39]. The specific capacitance values (389, 361, 352, 276, 233, and 131 F/g, respectively) for current densities ranging from 1 to 10 Ag^{-1} validated the electrode's robust behavior.

Scanning rates and current densities are shown by the relevant fluctuations in individual capacitance values in Fig. 4 (c) and (d). A lower specific capacitance is observed at higher scan rates owing to kinetic constraints on proton transport from the electrolyte to the electrode surface. Reduced rates of ion adsorption and desorption are the result. The specific capacitance drops down sharply as the discharge current density rises with increasing current values.

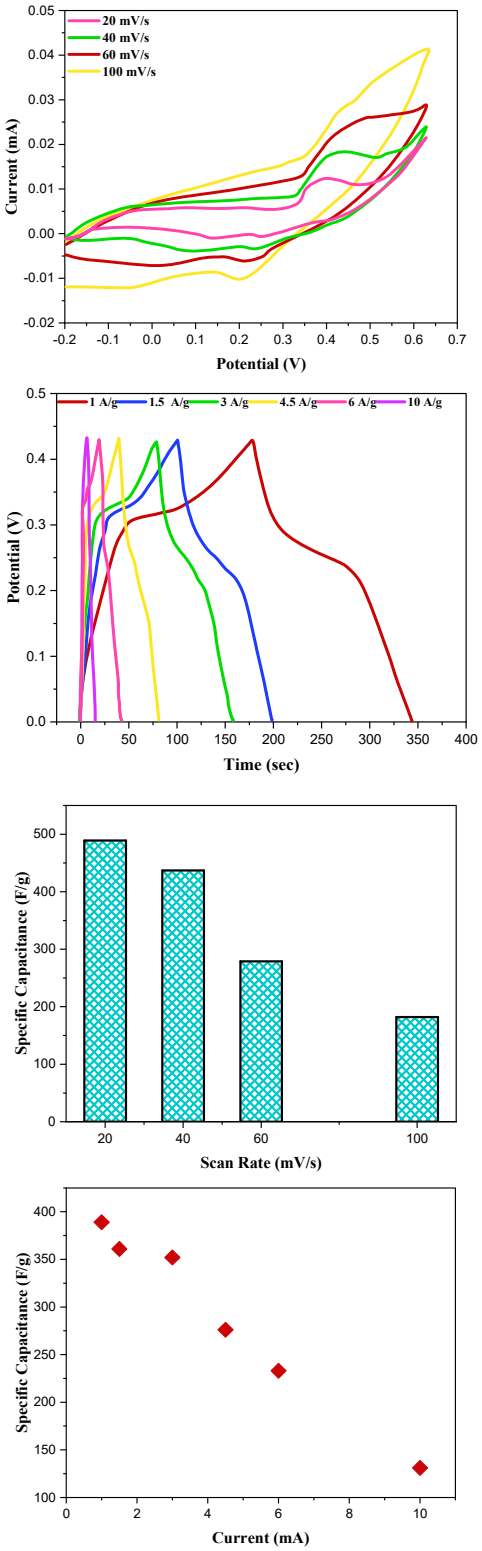

Figure 4. Plot for (a) evaluation of Scanning rate and Specific Capacitance, (b) evaluation of Current Density and Specific Capacitance, (c)CV, and(d)GCD.

Since the electrolyte and electrode surface do not have adequate time to undertake full Faradaic redox reactions, the higher resistance could be the reason behind this. Faradaic reactions dominate the electrochemical activity because Fe_2O_3 NRs in the water-based electrolyte indicate pseudocapacitive behavior. The pseudo capacitance can be caused by Mn+3/Mn+2 pair.

The cyclic stability of electrode was assessed by monitoring the charge-discharge potentials for 500 cycles at 6 Ag^{-1}, as depicted in Figure 5 (a). Surprisingly, the permeable Fe_2O_3 NRs retained an astounding 94% of their initial characteristics, demonstrating their exceptional durability and endurance, even after undergoing such lengthy cycling. A promising indicator of the material's long-term stability, the cycle stability test revealed that the form of the permeable Fe_2O_3 NRs remained unchanged. The fact that the shape of the permeable Fe_2O_3 nanorods does not alter once the cycling process is complete indicates that the Fe_2O_3 electrode did not experience any discernible structural changes. Despite the changing electrochemical conditions that are intrinsic to cycling, this discovery proves that the structural integrity of the electrode remains strong.

Due in large part to electrochemical impedance spectroscopy (EIS), the complex dynamics of electrochemical reactions became better understood. By employing a 10 mV amplitude signal that ranged from 1 Hz to 100 kHz, EIS was able to assess the ion mobility between the electrolyte and electrode surface. Figure 5 (b) illustrates the Nyquist curve before and after 500 sets of galvanostatic charge-discharge and it is shown exactly as it is. At higher frequencies, the Nyquist plot displays the ESR which we were able to measure by finding the intersects of the curve with real impedance axis.

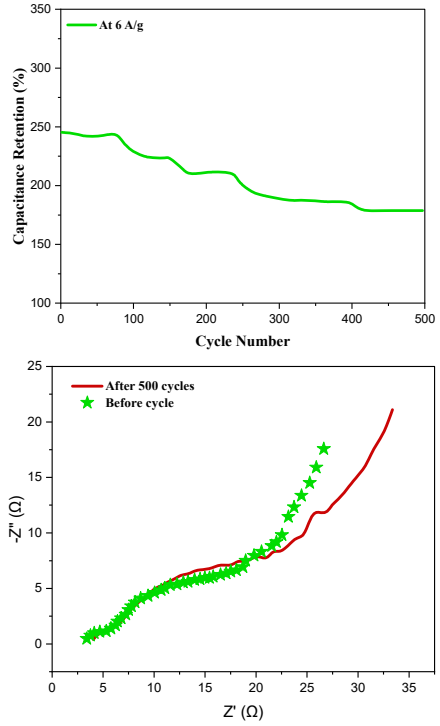

Figure 5 (a). The electrochemical impedance spectrum of Fe_2O_3 NRs and (b) the cyclic behaviour of Fe_2O_3 Nanorods at 6 A/g.

For permeable MnO NRs electrode, it is surprising that the ESR value stayed about the same from 3.22 Ω prior charge-discharging to 3.45 Ω subsequently 500 sets. Based on the EIS data, the sample of permeable Fe_2O_3 NRs seemed to have a lower electrolytic ion diffusion resistance and steeper slope in middle and lower frequency sections, suggesting a low sequence resistance (Rs = 3.2 Ω). on pages 28 and 29. The Rs value, which remains constant even after 500 GCD cycles, demonstrates that the electrode treated with Fe_2O_3 is exceptionally chemically stable, an important property for long-term supercapacitor applications. The specific capacitance performance is listed in Table 1.

Table 1. The specific capacitor results of the permeableFe_2O_3 NRs electrode.

S. No	Specimen	Electrolyte	No. of cycles (Retention) (%)	Csp (F/g)
1.	Fe 2O3	1 M of KOH	500 (94)	489

4. CONCLUSIONS

This study showcased the hydrothermal production of Fe_2O_3nanoparticles and provided insights into their structural and electrochemical characteristics. Confirming the crystalline clarity of the synthesized permeable Fe_2O_3 NRs, the materials exhibited a clearly specified cubic phase belonging to the Ia3 space group. Confirming the presence of Fe_2O_3 and offering further insight within the material's bonding states, extrapolative X-ray photoelectron spectroscopy (XPS) showed unique binding energies for Fe 2p and O 1s. The vibrations of metal oxides and other chemical linkages were used by FTIR to gain a deeper understanding the composition of the materials. By using Raman spectroscopy, we were able to confirm the structural stability of the Fe_2O_3 NRs by studying how morphological alterations affected their crystal structure. Electrochemical tests demonstrated the exceptional super capacitive performance of permeable Fe_2O_3 NRs. Using a 1 M KOH electrolyte solution and a scan rate of 10 mVs^{-1}, the specific capacitance was determined to be 489 F/g in CV investigations and 389 F/g in GCD testing. The Fe_2O_3 NRs' outstanding ion diffusion capabilities were highlighted by the EIS research, which found a minimal ESR of 3.26 Ω. Astonishingly, the Fe_2O_3 NRs retained 94% of their capacitor during 500 charge-discharge cycles. Because of its outstanding chemical stability, Fe_2O_3 treatments produce outstanding performance from electrodes. Overall, these results indicate that permeable Fe2O3 nanorods show promise as a material for upcoming technological supercapacitors.

REFERENCES

[1] F. Azimov and H. M. Jung, 2023 “Metal oxide nanomaterials for supercapacitor applications,” in *Advances in Electronic Materials for Clean Energy Conversion and Storage Applications*, , pp. 343–364.DOI:10.1016/B978-0-323-91206-8.00025-X

[2] M. C. Fite and T. Imae, 2021 “Capacitance enhancement

of nitrogen-doped graphene oxide/magnetite with polyaniline or carbon dots under external magnetic field: Supported by theoretical estimation," *J Colloid Interface Sci*, vol. 594, pp. 228–244. DOI: 10.1016/j.jcis.2021.02.112

[3] Fatma Mohamed Mahgoub1,2*, S. M. Al-Rashdi3, 2016 "Investigate the Corrosion Inhibition of Mild Steel in Sulfuric Acid Solution by Thiosemicarbazide," Journal of Physical Chemistry, vol. 6, pp. 54-66. DOI:10.4236/ojpc.2016.63006

[4] S. Venkatesa Prabhu, G. Ramesh, A. T. Adugna, S. M. Beyan, and K. Gizachew Assefa, 2019 "Kinetics of iron bioleaching using isolated leptospirillumferriphilum: Effect of temperature," *International Journal of Innovative Technology and Exploring Engineering*, vol. 8, no. 12, pp. 76–81. DOI: 10.35940/ijitee. L3210.1081219

[5] Mobasherpour, A.A. Tofigh, M. Ebrahimi, Effect of nano-size Al2O3 reinforcement on the mechanical behavior of synthesis 7075 aluminum alloy composites by mechanical alloying, Materials Chemistry and Physics, Volume 138, Issues 2–3, 2013, Pages 535-541,DOI:10.1016/j.matchemphys.2012.12.015.

[6] T. A. Amibo, S. M. Beyan, M. Mustefa, V. P. Sundramurthy, and A. B. Bayu, 2022 "Development of Nanocomposite based Antimicrobial Cotton Fabrics Impregnated by Nano SiO2 Loaded AgNPs Derived from Eragrostis Teff straw," *Materials Research Innovations*, vol. 26, no. 7, pp. 405–414. DOI:10.1080/14328917.2021.2022372

[7] Vijayakumar Arun, R. Kannan, S. Ramesh, M. Vijayakumar, P. S. Raghavendran, M. Siva Ramkumar, P. Anbarasu, Venkatesa Prabhu Sundramurthy, 2022 "Review on Li-Ion Battery vs Nickel Metal Hydride Battery in EV", Advances in Materials Science and Engineering, vol. 2022, Article ID 7910072, 7 pages. pages DOI:10.1155/2022/7910072

[8] S. Mayakannan, R. Rathinam, Rajasekaran Saminathan, R. Deepalakshmi, Mahesh Gopal, J. Justin Maria Hillary, S. Nanthakumar, V. Y. Ganvir, Pallavi Singh, 2022 "Analysis of Spectroscopic, Morphological Characterization and Interaction of Dye Molecules for the Surface Modification of TiB2 Nanoparticles", Journal of Nanomaterials, vol. 2022, Article ID 1033216, 9 pages. DOI: 10.1155/2022/1033216

[9] B. Ramesh, S. Sathish Kumar, A. H. Elsheikh, S. Mayakannan, K. Sivakumar, and S. Duraithilagar, 2022 "Optimization and experimental analysis of drilling process parameters in radial drilling machine for glass fiber/nano granite particle reinforced epoxy composites," in *Materials Today: Proceedings*, Elsevier Ltd, pp. 835–840. DOI:10.1016/j.matpr.2022.04.042

[10] B. Tessema, G. Gonfa, S. Mekuria Hailegiorgis, and S. Venkatesa Prabhu, 2023 "An Overview of Current and Prognostic Trends on Synthesis, Characterization, and Applications of Biobased Silica," *Advances in Materials Science and Engineering*, vol. 2023, DOI: 10.1155/2023/4865273

[11] Venkatramanan Varadharajan, Dilip Saravanan Senthilkumar, Kathiresan Senthilkumar, Venkatesa Prabhu Sundramurthy, Rahul Manikandan, Hariprasath Senthilarasan, Harish Ganesan, IndiravadananKesavamoorthy, Arulvel Ramasamy, 2022 "Process modeling and toxicological evaluation of adsorption of tetracycline onto the magnetized cotton dust biochar," *Journal of Water Process Engineering*, vol. 49. DOI: 10.1016/j.jwpe.2022.103046

[12] I. S. N. V. R. Prasanth, PrabaharJeevanandam, P. Selvaraju, K. Sathish, S. K. Hasane Ahammad, P. Sujatha, M. Kaarthik, S. Mayakannan, Bashyam Sasikumar, 2023 "Study of Friction and Wear Behavior of Graphene-Reinforced AA7075 Nanocomposites by Machine Learning," *J Nanomater*, vol. 2023. DOI:10.1155/2023/5723730

[13] P. Muruganandhan, S. Jothilakshmi, R. Vivek, S. Nanthakumar, S. Sakthi, S. Mayakannan, R. Girimurugan, 2023 "Investigation on silane modification and interfacial UV aging of flax fibre reinforced with polystyrene composite," *Mater Today Proc*. DOI: 10.1016/j.matpr.2023.03.272

[14] V. Balan, S. Ramakrishnan, G. Palani, and M. Selvaraju, 2024 "investigation on the enhancement of heat transferring counterflow double-pipe heat exchanger using nanofluids," *Thermal Science*, vol. 28, no. 1A, pp. 233–240. DOI: 10.2298/TSCI230312273V

[15] Mohanasundaram Sugumar, Varadharajan Venkatramanan, Selvaraju Mayakannan, Manikandan, Subbaiya Ramasamy, Jayakumar Mani, Sundaramurthy Venkatesa Prabhu, Gurunathan Baskar, Pugazhendhi Arivalagan, 2024 "Green ammonia as peerless entity for realm of clean-energy carrier toward zero carbon emission: Purviews, neoteric tendencies, potentialities and downsides," *Fuel*, vol. 365. DOI: 10.1016/j.fuel.2024.131118

[16] Roseline, S., Paramasivam, V., Parameswaran, P., Antony, A.G. (2019). Evaluation of mechanical properties and stability of Al 6061 with addition of ZrO2 And Al2O3. Journal of New Materials for Electrochemical Systems, Vol. 22, No. 1, pp. 21-23. DOI: 10.14447/jnmes.v22i1.a05.

[17] Min, Jiakang and Kierzek, Krzysztof and Chen, Xuecheng and Chu, Paul K. and Zhao, Xi and Kaleńczuk, Ryszard J. and Tang, Tao and Mijowska, Ewa, 2017 "Facile synthesis of porous iron oxide/graphene hybrid nanocomposites and potential application in electrochemical energy storage," *New Journal of Chemistry*, vol. 41, no. 22, pp. 13553–13559. DOI: 10.1039/C7NJ03416D

[18] Sathish, T., Chandramohan, D., Vijayan, V., Sebastian, P.J. (2019). Investigation on microstructural and mechanical properties of Cu reinforced with Sic composites prepared by microwave sintering process. Journal of New Materials for Electrochemical Systems, Vol. 22, No. 1, pp. 5-9. DOI: 10.14447/jnmes.v22i1.a02.

[19] Vicente de Oliveira Sousa Neto, Tiago Melo Freire, Gilberto Dantas Saraiva, Celio Rodrigues Muniz, Marcony Silva Cunha, Pierre Basílio Almeida Fechine, Ronaldo Ferreira do Nascimento, 2019 "Water Treatment

Devices Based on Zero-Valent Metal and Metal Oxide Nanomaterials," in *Nanomaterials Applications for Environmental Matrices: Water, Soil and Air*, pp. 187–225. DOI: 10.1016/B978-0-12-814829-7.00005-7

[20] J. J. William, I. M. Babu, and G. Muralidharan, 2019 "Lithium ferrite (α-LiFe5O8) nanorod based battery-type asymmetric supercapacitor with NiO nanoflakes as the counter electrode," *New Journal of Chemistry*, vol. 43, no. 38, pp. 15375–15388. DOI: 10.1039/C9NJ03774H

[21] Y. Wang, T. Zhang, X. Zheng, X. Tian, and S. Yuan, 2023 "Enhancing Energy Storage via Confining Sulfite Anions onto Iron Oxide/Poly(3,4-Ethylenedioxythiophene) Heterointerface," *ACS Appl Mater Interfaces*, vol. 15, no. 51, pp. 59413–59421. DOI: 10.1021/acsami.3c13148

[22] Thiyagarajan, K., Jayaraman, M., Vijayan, V., Ramkumar, R. (2020). Cluster analysis of lost foam casted Al-Zn-Mg-Cu alloy with K–Mean algorithm. Journal of New Materials for Electrochemical Systems, Vol. 23, No. 1, pp. 45-51. DOI: 10.14447/jnmes.v23i1.a09.

[23] Kong, LB, Que, W, Liu, L, Boey, FYC, Xu, ZJ, Zhou, K, Li, S, Zhang, T & Wang, C 2018, Oxide based supercapacitors: I-manganese oxides. in LB Kong (ed.), Nanomaterials for Supercapacitors. CRC Press, pp. 162-276. DOI: 10.1201/9781315153025-4

[24] M. Aghazadeh, I. Karimzadeh, and M. R. Ganjali, 2017 "Electrochemical evaluation of the performance of cathodically grown ultra-fine magnetite nanoparticles as electrode material for supercapacitor applications," *Journal of Materials Science: Materials in Electronics*, vol. 28, no. 18, pp. 13532–13539. DOI: 10.1007/s10854-017-7192-z

[25] Y.-C. Chen, J.-H. Hsu, Y.-G. Lin, and Y.-K. Hsu, 2017 "Synthesis of Fe_2O_3 nanorods/silver nanowires on coffee filter as low-cost and efficient electrodes for supercapacitors," *Journal of Electroanalytical Chemistry*, vol. 801, pp. 65–71. DOI: 10.1016/j.jelechem.2017.07.032

[26] S. Tanwar, A. Arya, and A. L. Sharma, 2023 "MoSe2-FeOOH nanocomposite as hybrid electrode material for high-performance symmetric supercapacitor," *Mater Res Bull*, vol. 160. DOI: 10.1016/j.materresbull.2022.112144

[27] Yuxue Wei, Ruimin Ding, Chenghua Zhang, BaoliangLv, Yi Wang, Chengmeng Chen, Xiaoping Wang, Jian Xu, Yong Yang, Yongwang Li, 2017 "Facile synthesis of self-assembled ultrathin α-FeOOH nanorod/graphene oxide composites for supercapacitors," *J Colloid Interface Sci*, vol. 504, pp. DOI: 10.1016/j.jcis.2017.05.112

[28] Abolanle S. Adekunle, Bolade O. Agboola, Kenneth I. Ozoemena, Eno E. Ebenso, John A.O. Oyekunle, Oluwafemi S. Oluwatobi, Joel N. Lekitima, 2015 "Comparative supercapacitive properties of asymmetry two electrode coin type supercapacitor cells made from MWCNTS/cobalt oxide and MWCNTs/iron oxide nanocomposite," *Int J Electrochem Sci*, vol. 10, no. 4, pp. 3414–3430. DOI: 10.1016/S1452-3981(23)06550-1

[29] Yu, Shijin and Hong Ng, Vincent Ming and Wang, Fajun and Xiao, Zhuohao and Li, Cuiyun and Kong, Ling Bing and Que, Wenxiu and Zhou, Kun, 2018 "Synthesis and application of iron-based nanomaterials as anodes of lithium-ion batteries and supercapacitors," *J Mater Chem A Mater*, vol. 6, no. 20, pp. 9332–9367. DOI: 10.1039/C8TA01683F

[30] Wanyi Xie, Yanzi Wang, Jie Zhou, Meng Zhang, Jiali Yu, Caizhen Zhu, Jian Xu, 2020 "MOF-derived CoFe2O4 nanorods anchored in MXene nanosheets for all pseudocapacitive flexible supercapacitors with superior energy storage," *Appl Surf Sci*, vol. 534. DOI: 10.1016/j.apsusc.2020.147584

[31] R. Kumar, R. K. Singh, A. R. Vaz, R. Savu, and S. A. Moshkalev, 2017, "Self-Assembled and One-Step Synthesis of Interconnected 3D Network of Fe3O4/Reduced Graphene Oxide Nanosheets Hybrid for High-Performance Supercapacitor Electrode," *ACS Appl Mater Interfaces*, vol. 9, no. 10, pp. 8880–8890. DOI: 10.1021/acsami.6b14704

[32] D. M. G. T. Nathan and S. J. M. Boby, 2017 "Hydrothermal preparation of hematite nanotubes/reduced graphene oxide nanocomposites as electrode material for high performance supercapacitors," *J Alloys Compd*, vol. 700, pp. 67–74. DOI: 10.1016/j.jallcom.2017.01.070

[33] M. Boufas, O. Guellati, A. Harat, D. Momodu, J. Dangbegnon, N. Manyala& M. Guerioune, 2020 "Optical and electrochemical properties of iron oxide and hydroxide nanofibers synthesized using new template-free hydrothermal method,"*J Nanostructure Chem*, vol. 10, no. 4, pp. 275–288. DOI: 10.1007/s40097-020-00348-8

[34] Ruizhi Li, Yimeng Wang, Cheng Zhou, Chong Wang, Xin Ba, Yuanyuan Li, Xintang Huang and Jinping Liu, 2015 "Carbon-Stabilized High-Capacity Ferroferric Oxide Nanorod Array for Flexible Solid-State Alkaline Battery-Supercapacitor Hybrid Device with High Environmental Suitability," *Adv Funct Mater*, vol. 25, no. 33, pp. 5384–5394. DOI: 10.1002/adfm.201502265

[35] Jiawei Zhou, Chao Zhang, Taoxia Niu, RenxingHuang, Shuang Li, Jin Z. Zhang, and Jingguang G. Chen, 2018, "Controlled Synthesis of Fe3O4 Nanospheres Coated with Nitrogen-Doped Carbon for High Performance Supercapacitors," *ACS Appl Energy Mater*, vol. 1, no. 9, pp. 4599–4605. DOI: 10.1021/acsaem.8b00770

[36] K. Bramhaiah, I. Pandey, V. N. Singh, N. Kambhala, S. Angappane, and N. S. John, 2018 "Films and dispersions of reduced graphene oxide based Fe_2O_3 nanostructure composites: Synthesis, magnetic properties and electrochemical capacitance," *Mater Chem Phys*, vol. 209, pp. 1–9. DOI: 10.1016/j.matchemphys.2018.01.057

[37] S.Dinesh, A.Godwin Antony, S.Karuppusamy, V.Vijayan and B.Suresh Kumar, 2016. Experimental investigation and optimization of machining parameters in CNC turning operation of duplex stainless steel. Asian Journal of Research in Social Sciences and Humanities 6,pp. 179-195. DOI: 10.5958/2249-7315.2016.01006.6

[38] S.Dinesh, A.Godwin Antony, K.Rajaguru and V.Vijayan. 2016. Experimental investigation and optimization of material removal rate and surface roughness in CNC turning of EN24 alloy steel, Mechanics and Mechanical Engineering, 20 (4) 451—466. DOI: 10.5958/2249-

7315.2016.00654.7
[39] T.Tamizharasan, N.Senthil Kumar, V.Selvkumar, S.Dinesh, 2019. Taguchi's Methodology of optimizing turning parameters over chip thickness ratio in machining PM AMMC, SN Appl. Sci. 1: 160., Springer Publishers. DOI: 10.1007/s42452-019-0170-8